4-1-2020

The Surface Termination of CsPbBr3 Perovskite Quantum Dots Determined by Solid-State NMR Spectroscopy

Yunhua Chen
Iowa State University and Ames Laboratory, ychen007@iastate.edu

Sara R. Smock
University of Southern California

Anne H. Flintgruber
Ames Laboratory

Frédéric A. Perras
Ames Laboratory, fperras@ameslab.gov

Richard L. Brutchey
University of Southern California

See next page for additional authors

The Surface Termination of CsPbBr3 Perovskite Quantum Dots Determined by Solid-State NMR Spectroscopy

Abstract

Cesium lead halide perovskite quantum dots (QDs) have gained significant attention as next-generation optoelectronic materials; however, their properties are highly dependent on their surface chemistry. The surfaces of cuboidal CsPbBr3 QDs have been intensively studied by both theoretical and experimental techniques, but fundamental questions still remain about the atomic termination of the QDs. The binding sites and modes of ligands at the surface remain unproven. Herein, we demonstrate that solid-state NMR spectroscopy allows the unambiguous assignments of organic surface ligands via 1H, 13C, and 31P NMR. Surface-selective 133Cs solid-state NMR spectra show the presence of an additional 133Cs NMR signal with a unique chemical shift that is attributed to Cs atoms terminating the surface of the particle and which are likely coordinated by carboxylate ligands. Dipolar dephasing curves that report on the distance between the surface ammonium ligands and Cs and Pb were recorded using double resonance 1H{133Cs} and 1H{207Pb} RESPDOR experiments. Model QD surface slabs with different possible surface terminations were generated from the CsPbBr3 crystal structure and theoretical RESPDOR dipolar dephasing curves considering all possible 1H-133Cs/207Pb spin pairs were then calculated. Comparison of the calculated and experimental RESPDOR curves indicates the particles are CsBr terminated (not PbBr2 terminated), with alkylammonium ligands situated within surface Cs vacancies, consistent with the surface-selective 133Cs NMR experiments. These results highlight the utility of high-resolution solid-state NMR spectroscopy for studying ligand binding and the surface structure of nanomaterials.

Keywords

Nanoparticles, Semiconductors, Materials Science, NMR Spectroscopy, Surface Chemistry

Disciplines

Materials Chemistry | Nanoscience and Nanotechnology

Authors

Yunhua Chen, Sara R. Smock, Anne H. Flintgruber, Frédéric A. Perras, Richard L. Brutchey, and Aaron J. Rossini

The Surface Termination of $CsPbBr_3$ Perovskite Quantum Dots Determined by Solid-State NMR Spectroscopy

Yunhua Chen,[1, 2] Sara R. Smock,[3] Anne H. Flintgruber,[1] Frédéric A. Perras,[1] Richard L. Brutchey,[3*] Aaron J. Rossini[1, 2*]

1. U.S. DOE Ames Laboratory, Ames, IA 50011 (USA)

2. Department of Chemistry, Iowa State University, Ames, IA 50011 (USA)

3. Department of Chemistry, University of Southern California, Los Angeles, CA 90089 (USA)

KEYWORDS: Nanoparticles, Semiconductors, Materials Science, NMR Spectroscopy, Surface Chemistry

ABSTRACT: Cesium lead halide perovskite quantum dots (QDs) have gained significant attention as next-generation optoelectronic materials; however, their properties are highly dependent on their surface chemistry. The surfaces of cuboidal $CsPbBr_3$ QDs have been intensively studied by both theoretical and experimental techniques, but fundamental questions still remain about the atomic termination of the QDs. The surface binding sites and modes of ligands at the surface remain unproven. Herein, we demonstrate that solid-state NMR spectroscopy allows the unambiguous assignment of organic surface ligands via ^{1}H, ^{13}C, and ^{31}P NMR. Surface-selective ^{133}Cs solid-state NMR spectra show the presence of an additional ^{133}Cs NMR signal with a unique chemical shift that is attributed to Cs atoms terminating the surface of the particle and which are likely coordinated by carboxylate ligands. Dipolar dephasing curves that report on the distance between the surface ammonium ligands and Cs and Pb were recorded using double resonance $^{1}H\{^{133}Cs\}$ and $^{1}H\{^{207}Pb\}$ RESPDOR experiments. Model QD surface slabs with different possible surface terminations were generated from the $CsPbBr_3$ crystal structure and theoretical RESPDOR dipolar dephasing curves considering all possible ^{1}H-$^{133}Cs/^{207}Pb$ spin pairs were then calculated. Comparison of the calculated and experimental RESPDOR curves indicates the particles are CsBr terminated (not $PbBr_2$ terminated) with alkylammonium ligands substituting into some surface Cs sites, consistent with the surface-selective ^{133}Cs NMR experiments. These results highlight the utility of high-resolution solid-state NMR spectroscopy for studying ligand binding and the surface structure of nanomaterials.

INTRODUCTION

Colloidal all-inorganic cesium lead halide perovskite ($CsPbX_3$, X = Cl, Br, or I) quantum dots (QDs) are intensively studied as a result of their excellent optoelectronic properties including tunable band gaps, high photoluminescence quantum yields (PLQY), narrow emission linewidths, suppressed blinking, and high defect tolerance.[1-3] These properties have led to a large variety of promising applications, such as light-emitting diodes (LEDs),[4,5] displays,[6] solar cells,[7] and lasers.[8] To date, the record certified cesium lead halide QD-based solar cells have demonstrated a power conversion efficiency of 16.6%.[9]

The optoelectronic properties of QDs are highly dependent on their surface coordination chemistry.[10-14] For instance, surface ligands play a critical role in passivating mid-gap electronic trap states and enabling high PLQY.[10, 11, 13, 15] Judicious selection of surface ligands can improve stability[16] and improve the quality of lead halide perovskite thin films formed from deposition of QD precursors.[17] Surface reconstruction, as well as ligand absorption-desorption, happen frequently at the surface of colloidal $CsPbBr_3$ QDs due to their intrinsically ionic and highly dynamic nature.[18, 19] Therefore, developing an atomistic description of the surface structure of $CsPbX_3$ QDs is of paramount importance. Previously, the thermodynamics of ligand binding to $CsPbBr_3$ QDs were extensively studied by solution ^{1}H NMR spectroscopy.[20] It was shown that oleic acid and dodecylamine native ligands dynamically interact with the surface with ligand densities of 2.4-3.0 ligand nm^{-2}. Titration of 10-undecenylphosphonic acid into a colloidal $CsPbBr_3$ QDs suspension results in irreversible tight binding of phosphonate by replacement of the native oleate. The stronger phosphonate ligand binding results in improved surface passivation and higher PLQY.[20] Fundamental questions still remain, however, regarding the ligand coordination chemistry at the QD surface and how the surface is terminated.[21-23]

Bodnarchuk *et al.* previously used DFT calculations to calculate different possible surface terminations of $CsPbBr_3$ QDs and predict the effects of different surface terminations on the electronic structures and resulting optoelectronic properties.[22] They proposed that freshly prepared, highly luminescent cuboidal $CsPbBr_3$ QDs have a structure described as $[CsPbBr_3](PbBr_2)\{AX'\}$, which corresponds to a $CsPbBr_3$ core terminated by a $PbBr_2$ inner shell and an outer shell composed of monovalent cations (A = Cs^+ or ammonium ligands) and anions (X' = Br^- and carboxylic acid ligands).[22] The $PbBr_2$ terminated surface $[CsPbBr_3](CsBr)\{PbBr_2\}$ was thought to be highly unlikely because of the energetically unfavorable distortion of the Pb^{2+} octahedral coordination

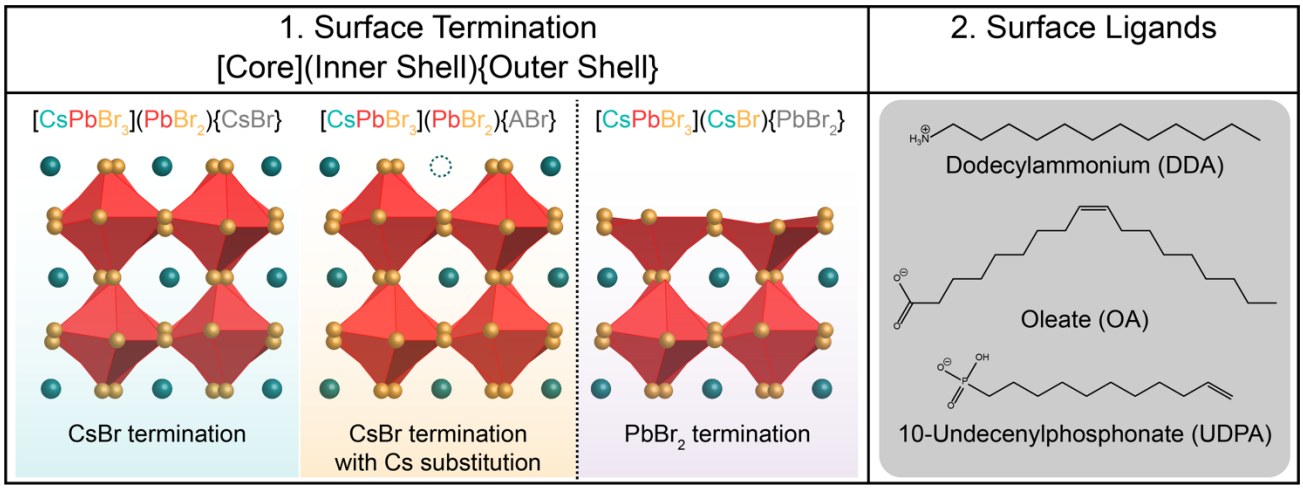

Figure 1. Idealized models of the surface termination of the as-synthesized orthorhombic $CsPbBr_3$ QDs. Cs, Br atoms are depicted by blue and yellow spheres, respectively. Pb atoms reside at the center of the red octahedra formed by Br. The QDs consist of an inorganic core with CsBr (left) or $PbBr_2$ (right) surface termination. Substitution of a surface Cs atom with an ammonium ligand gives an ABr terminated surface (A = Cs or DDA, middle left). Both surfaces are capped by cationic and anionic organic ligands at the outermost layer. The anionic X-type oleic acid and UDPA ligands are assumed to bind to exposed Cs or Pb surface atoms.

and the high density of X-type ligands, such as oleic acid, required to passivate those surface Pb atoms.[22] This termination is also predicted to promote the formation of charge-trap sites after only 25% ligand loss.[22] Physical evidence regarding the termination of these QDs is still lacking and experimental methods are needed to prove whether as-synthesized $CsPbX_3$ QDs are terminated with $PbBr_2$ layers or AX layers (where A is Cs or alkylammonium). The positions of the organic ligands on the QD surfaces are also unknown.

Normally, electron microscopy, spectroscopy, X-ray diffraction or scattering methods are used to characterize $CsPbX_3$ QDs. However, these techniques provide limited structural information about the surface of the QDs because the surfaces are inherently disordered and highly dynamic. Since all elements of cesium lead halide perovskites have accessible NMR active nuclei, solid-state NMR is potentially an ideal technique for this task. Chemical shifts are very sensitive to the local chemical environment of a given nucleus and the measurements of scalar and dipolar couplings between nuclear spins provide valuable connectivity and/or proximity information.[24-29] Indeed, solid-state NMR spectroscopy has proven to be a valuable tool to study cation dynamics[30-35] and the structure of bulk lead halide perovskites.[31, 36-42] To the best of our knowledge, solid-state NMR spectroscopy has only been applied to study lead halide perovskite QDs in a handful of cases. Piveteau *et al.*[43] recorded DNP enhanced spectra of ^{133}Cs from perovskite $CsPbBr_3$ QDs. In addition, Brown *et al.*[44] have recently applied 2D solid-state ^{1}H-^{31}P solid-state NMR experiments to probe the binding of octylphosphonate ligands to $CsPbBr_3$ QDs. However, these studies have not provided direct information on the surface termination of $CsPbBr_3$ QDs. Here, solid-state NMR spectroscopy is applied to characterize the surface of precipitated cuboidal $CsPbBr_3$ QDs passivated with dodecylammonium, oleate, and 10-undecenylphosphonate ligands. Notably, surface-selective ^{133}Cs and ^{207}Pb solid-state NMR experiments suggest that the surface of the cuboidal $CsPbBr_3$ particles are terminated by a CsBr shell, with (Figure 1). $^{1}H\{^{133}Cs\}$ and $^{1}H\{^{207}Pb\}$ RESPDOR measurement confirm this proposition and further suggest that alkylammonium ligands substitute into Cs sites at the surface of the particles.

RESULTS AND DISCUSSION

The $CsPbBr_3$ QDs used in this study were synthesized using a modified version of the hot-injection synthesis initially reported by Protesescu *et al.*[1] Here, dodecylamine was substituted for oleylamine to avoid alkenyl proton overlap with oleic acid and diphenyl ether is substituted for 1-octadecene to avoid vinylic proton overlap with 10-undecenylphosphonic acid in the ^{1}H NMR spectra (*vide infra*). The resulting QDs possess a native ligand shell comprised of dodecylammonium and oleate that dynamically bind to the QD surface.[19, 20] The solution ^{1}H NMR spectrum of the as-synthesized QDs clearly shows the diagnostic alkenyl protons of oleic acid in the chemical shift window of δ = 5.4-5.8 ppm, with the resonance for bound oleate being broadened and shifted downfield relative to that of free oleic acid (Figure S1). Based on the concentration of $CsPbBr_3$ QDs determined by UV-vis spectroscopy, and integration of the bound alkenyl resonance of oleate against an internal standard in the solution ^{1}H NMR spectrum, the bound oleate ligand density was calculated to be 0.62 oleate nm^{-2} (see Supporting Information).[19] However, from the solution ^{1}H NMR spectra it is difficult to estimate the relative concentration dodecylammonium ligands due to overlap of residual solvent and ligand signals. Integration of the ammonium and oleic acid vinyl signals in the 50 kHz MAS ^{1}H spin echo spectrum indicates a dodecylammonium to oleate ratio of roughly 1.7:1 (see Figure 2A and discussion of ^{1}H solid-state NMR spectra below). Using this ratio and the oleic acid ligand density from solution ^{1}H NMR we obtain an ammonium ligand density of 1.0 dodecylammonium nm^{-2} and an overall ligand density of 1.7 ligands nm^{-2}. This ligand density is less than the theoretical monolayer coverage of 5.8 ligands nm^{-2} previously estimated for $CsPbBr_3$.[19] However, this prior theoretical ligand density was calculated assuming that the surface is solely passivated by Cs and Br anions. Organic ligands such as oleic acid and alkyl ammoniums have much larger footprints on the order of 0.3–0.5 nm^2 ligand^{-1},[20, 45]

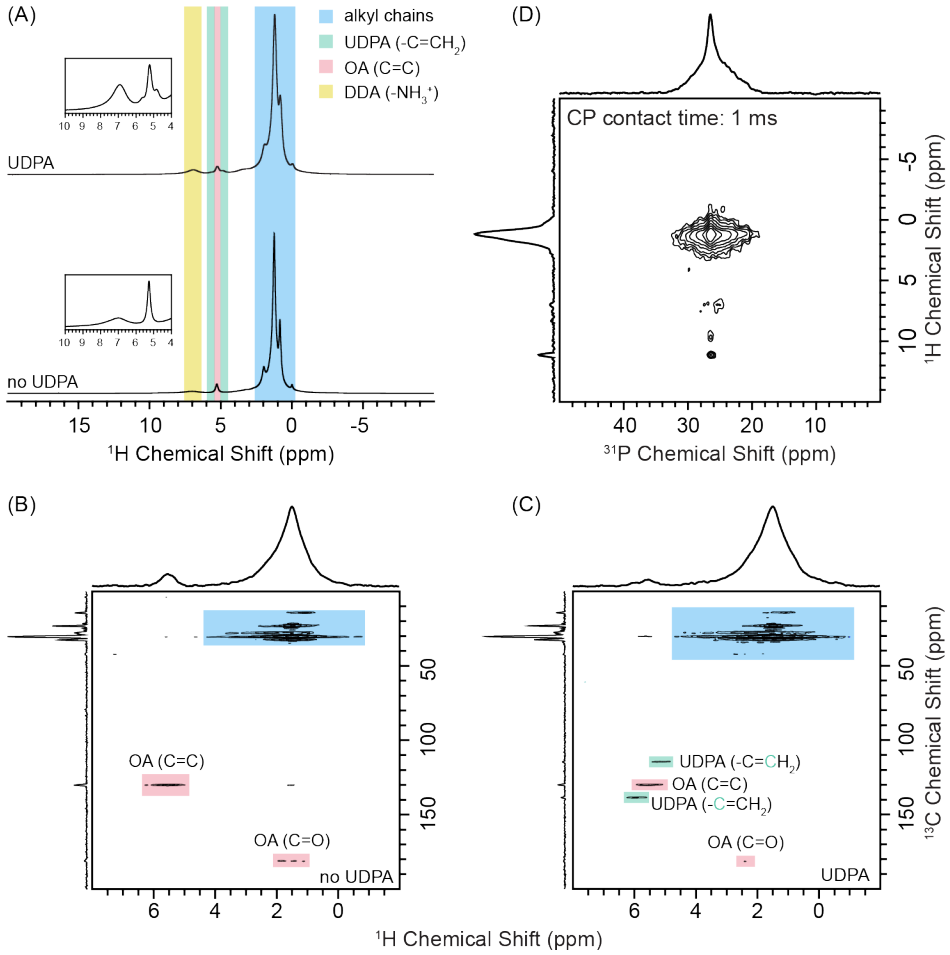

Figure 2. (A) MAS ^{1}H spin echo solid-state NMR spectra of $CsPbBr_3$ QDs with and without 10-undecenylphosphonate (UDPA). The insets show the diagnostic high-frequency chemical shifts of the vinyl functional groups of UDPA, alkenyl protons of oleate (OA), and the ammonium group of dodecylammonium (DDA). ^{1}H detected 2D dipolar ^{1}H-^{13}C CP-HETCOR spectra of $CsPbBr_3$ QDs (B) without and (C) with UDPA. (D) 2D dipolar ^{1}H→^{31}P CP HETCOR of $CsPbBr_3$ QDs with 10-undecenylphosphonate (UDPA). The CP contact time is indicated. All spectra were obtained with a 25 kHz MAS frequency.

hence, the maximum total ligand density should be on the order of 2–3 ligands nm^{-2}, in reasonable agreement with the measured values. A ligand density of 1.7 ligands nm^{-2} is fully consistent with the surface models proposed below.

A fraction of the as-synthesized $CsPbBr_3$ QDs was treated with 10-undecenylphosphonic acid during QD purification to perform a partial exchange of the native oleate ligands on the surface for the phosphonate ligand.[20] After treatment with 10-undecenylphosphonic acid, the solution ^{1}H NMR spectrum of the $CsPbBr_3$ QDs shows clear resonances for the distinct vinylic protons of bound phosphonate at δ = 5.2 and 6.0 ppm, with no evidence of free phosphonic acid in solution (Figure S1), confirming that the phosphonic acid binds irreversibly to the surface.[20] The relative amount of oleic acid that becomes liberated from the QD surface upon phosphonate binding is 0.7:1 (mol/mol). The ^{1}H solid-state NMR spectrum (Figure 2A) indicates the dodecylammoium to acid ligand ratio drops from 1.7:1 to 1.3:1 after 10-undecenylphosphonic acid exchange, suggesting that on average, more phosphonates bind than oleic acid is exchanged off.

Powder X-ray diffraction (PXRD) confirms that $CsPbBr_3$ QDs crystallize in the expected *Pnma* orthorhombic structure (Figure S2).[46] TEM shows that the QDs possess a cuboidal morphology with average edge lengths of 9.6 ± 1.3 and 8.9 ± 1.4 nm for QDs that have and have not undergone ligand exchange with 10-undecenylphosphonic acid, respectively (Figure S3). This is in qualitative agreement with QD sizes calculated using the photoluminescence emission spectra for $CsPbBr_3$ with phosphonate (10.5 nm, λ_{max} = 512 nm) and without phosphonate (9.3 nm, λ_{max} = 508 nm, Figure S4).[47] The QDs solutions were dried overnight under vacuum at room temperature and the precipitated QDs were used for solid-state NMR experiments.

We began our investigation of the surface structures of $CsPbBr_3$ QDs with ^{1}H solid-state NMR experiments since these experiments provide the highest sensitivity and can differentiate diagnostic functional groups of the surface ligands. Prior to ligand exchange with 10-undecenylphosphonic acid the main observable NMR signal covers a chemical shift range of ca. 0 to 2.5 ppm and corresponds to protons within the long aliphatic alkyl chain of the native dodecylammonium and oleate ligands (Figure 2A). The signal that resonates at ca. 5.3 ppm is attributed to the alkenyl protons from oleate. The broad signal centered at ca. 7.0 ppm is assigned to ammonium protons from dodecylammonium. This assignment was confirmed with ^{1}H{^{14}N} RESPDOR[48] experiments

that showed ^{14}N dipolar dephasing for these ^{1}H signals (see Figure S5 and Figure S6). Note that the ammonium ^{1}H NMR signals are hard to observe in our ^{1}H solution NMR experiments,[20] because of overlap with the signals from residual toluene. There are two additional ^{1}H NMR signals at ca. 4.9 and 5.7 ppm (Figure 2A) observed in the spectrum of the $CsPbBr_3$ QDs that were ligand exchanged with 10-undecenylphosphonic acid. These signals are assigned to distinct vinylic protons from the UPDA ligands. These chemical shifts are consistent with those observed in the solution ^{1}H NMR spectrum of a $CsPbBr_3$ QD suspension. The ^{1}H spin echo solid-state NMR spectra confirm binding of dodecylammonium, oleate, and 10-undecenylphosphonate to the $CsPbBr_3$ QD surface.

2D double-quantum single-quantum (DQ-SQ) dipolar ^{1}H-^{1}H homonuclear correlation experiments[49-51] show the expected correlations for the different surface ligand groups, helping to confirm the ^{1}H NMR signal assignments (Figure S7, and accompanying discussion in the SI). The assignments of ^{1}H NMR signals of the surface ligands were also confirmed with ^{1}H→^{13}C cross-polarization magic angle spinning (CPMAS) and proton detected 2D ^{1}H{^{13}C} CP-HETCOR NMR spectra[52] (Figures 2B, 2C and Figure S8). The 1D and 2D ^{13}C solid-state NMR spectra show all of the resonances expected for dodecylammonium, oleate, and/or 10-undecenylphosphonate. The $-NH_3^+$ dodecylammonium ^{1}H NMR signals are likely absent from the 2D ^{1}H{^{13}C} CP HETCOR spectra because the ammonium protons are distant from most carbon atoms.

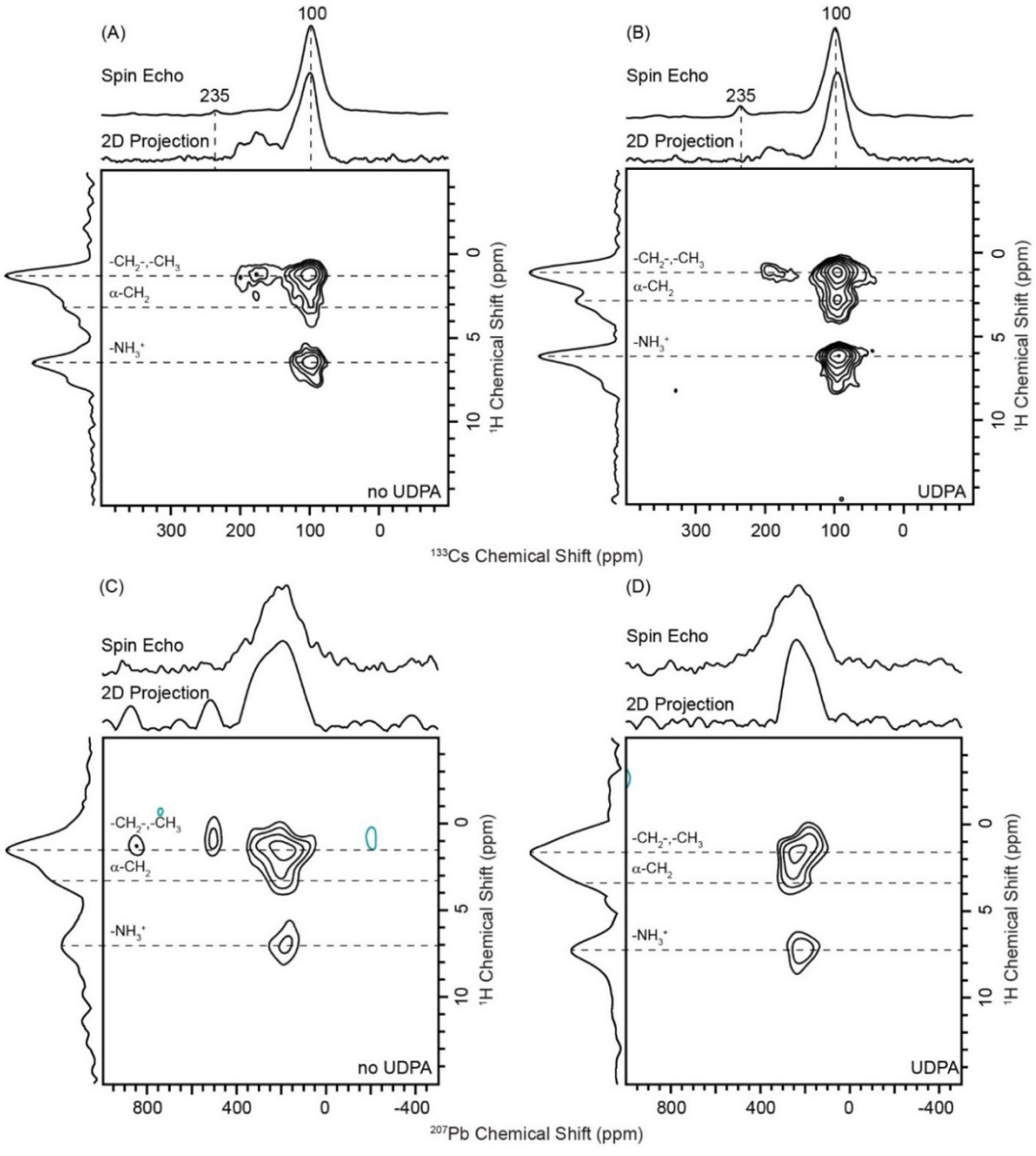

Figure 3. ^{133}Cs spin echo and 2D ^{1}H→^{133}Cs CP-HETCOR NMR spectra of $CsPbBr_3$ QDs (A) without and (B) with 10-undecenylphosphonic acid (UDPA). ^{207}Pb spin echo NMR spectra and 2D ^{207}Pb→^{1}H CP-HETCOR of $CsPbBr_3$ QDs (C) without and (D) with UDPA. The CP contact times were 9 ms and 8 ms for ^{133}Cs and ^{207}Pb CP-HETCOR experiments, respectively. The ^{207}Pb NMR signals at 500 ppm and 850 ppm are not real and are from t_1-noise.

A $^{1}H \rightarrow ^{31}P$ CP-HETCOR experiment was performed to identify potential binding sites for 10-undecenylphosphonate (UDPA) on the $CsPbBr_3$ QD surface and understand why ligand exchange with 10-undecenylphosphonate can enhance optical properties. Recently, Matthews and co-workers reported the ^{31}P solid-state NMR spectra of octylphosphonic acid capped $CsPbBr_3$ QDs and observed a primary ^{31}P peak at 25 ppm.[44] On the basis of the ^{31}P chemical shifts[53, 54] and the HETCOR experiments, this peak was assigned to singly deprotonated, monoanionic surface phosphonate groups. Holland *et al.* observed that SnO_2 particles capped with 2-carboxyethanephosphonic acid gave rise to broad ^{31}P NMR signals with similar chemical shift. They ascribed the broadening of signals to the presence of bi- and tri-dentate di-anionic surface phosphonate groups.[55] However, di-anionic phosphonates should resonate at ca. 15 ppm.[44, 53, 54]

The 2D ^{1}H-^{31}P HETCOR spectrum of $CsPbBr_3$ QDs with 10-undecenylphosphonate shows an intense, relatively narrow ^{31}P NMR signal at 26 ppm, and there is also a broader signal that extends to 20 ppm (Figure 2D). The peak at 26 ppm is assigned to singly deprotonated, monoanionic phosphonate because it correlates to high-frequency ^{1}H NMR peaks at ca. 9.5 ppm and 11 ppm that should correspond to acid protons.[44] The narrowing of the ^{31}P peak at 26 ppm could arise because a singly deprotonated phosphonic acid may coordinate to the surface in a monodentate fashion, permitting rotation that could help to average inhomogeneous broadening. The presence of two acid ^{1}H NMR signals suggest that there are distinct binding sites on the surface for the monoanionic 10-undecenylphosphonate. A part of the broader ^{31}P resonance correlates to ^{1}H NMR signals at ca. 7.5 ppm, which should correspond to the $-NH_3^+$ protons. This correlation would suggest that at least some of the surface phosphonates are ion paired with the positively charged ammonium ligands on the QD surface.

^{133}Cs direct excitation (spin echo) and surface-selective 2D dipolar $^{1}H \rightarrow ^{133}Cs$ CP-HETCOR NMR experiments were performed to obtain more definitive information about possible surface terminations of the QDs (Figure 3A and 3B). It has previously been shown that ^{133}Cs isotropic chemical shifts are sensitive probes of structure for bulk cesium lead halide perovskites and other related inorganic cesium phases.[36, 42, 56] The ^{133}Cs spin echo NMR spectra show signals from all Cs species present in the sample, including Cs in the bulk of the QD, surface Cs sites, and Cs in inorganic impurity phases. The intense ^{133}Cs NMR signal at 100 ppm is attributed to Cs ions in the bulk of $CsPbBr_3$ because this peak has the highest intensity and a similar chemical shift was reported in prior studies of microcrystalline $CsPbBr_3$.[42, 43, 56] The chemical shift of the very low intensity ^{133}Cs NMR signal at ca. 235 ppm is assigned to a small amount of Cs_4PbBr_6.[42] The broad, low-intensity ^{133}Cs NMR signal centered at ca. 170 ppm is attributed to Cs that resides on the surface of the QDs. Consistent with this hypothesis, the signal at 170 ppm attributed to surface Cs shows higher relative intensity in a 2D $^{1}H \rightarrow ^{133}Cs$ CP-HETCOR spectrum (Figure 3 and Figure S9). This unique ^{133}Cs chemical shift could occur because these sites may be coordinated by carboxylate or phosphonate ligands. As expected, the ^{133}Cs signals assigned to surface Cs atoms show higher relative intensity in short contact time $^{1}H \rightarrow ^{133}Cs$ CP-HETCOR spectra (Figure S10). Kovalenko and co-workers obtained a DNP-enhanced $^{1}H \rightarrow ^{133}Cs$ CPMAS spectrum of $CsPbBr_3$ QDs.[43] Consistent with the ^{133}Cs NMR spectra shown here, they observed ^{133}Cs NMR signals at ca. 170 ppm and 100 ppm, with the signal at 170 ppm showing high relative intensity in the CPMAS spectrum. However, a broad and intense signal centered at 0 ppm was also observed.[43] Cs cations in aqueous solution resonate at 0 ppm, hence, we speculate their signal may have arisen from Cs^+ dissolved in water dissolved in the DNP solvent or in the mesoporous silica used to disperse the particles.

The ^{1}H dimension of the 2D $^{1}H \rightarrow ^{133}Cs$ CP-HETCOR spectrum shows signals from the ligand including $-NH_3^+$ (δ = 6.5 ppm), CH_2 groups adjacent to the carboxylate group of the oleate anions (α-CH_2, δ = 3.0 ppm), and the CH_2 groups further along the alkyl chain (δ = 1.2 ppm). The enhanced relative intensity of the $-NH_3^+$ and α-CH_2 ^{1}H NMR signals in the projection of the HETCOR spectrum as compared to the ^{1}H spin echo spectrum is expected. These groups should be directly adjacent to the surface of the $CsPbBr_3$ QDs and hence more strongly dipole coupled to surface and bulk-like, sub-surface Cs atoms. If surface Cs atoms are coordinated by oleate or 10-undecenylphosphonate then they will be > 5.0 Å away from ammonium groups (this is confirmed by $^{1}H\{^{133}Cs\}$ RESPDOR experiments, see Figure 4 and discussion below). Therefore, the surface Cs atoms should show the most intense correlations to CH_2 signals of the oleate or 10-undecenylphosphonate alkyl chains.

^{207}Pb solid-state NMR experiments were also performed. The direct excitation ^{207}Pb spin echo spectrum shows a single broad peak centered at ca. 200 ppm. The 200 ppm chemical shift of $CsPbBr_3$ observed here is similar to the shift of 400 ppm reported for bulk $MAPbBr_3$,[37] and the shift of ca. 250 ppm reported for bulk $CsPbBr_3$.[42] Surface-selective ^{207}Pb NMR spectra were recorded by using proton detected $^{207}Pb \rightarrow ^{1}H$ CP-HETCOR experiments.[40, 52] Proton detection provides a significant sensitivity gain, allowing the observation of the fraction of ^{207}Pb that is proximate to the surface ligands.[40, 52] Even with ^{1}H detection these experiments were challenging and each required between 6 and 9 h of spectrometer time. Notably, the ^{207}Pb projection from the surface-selective 2D $^{207}Pb \rightarrow ^{1}H$ CP-HETCOR spectrum is similar to the ^{207}Pb spin echo spectrum, suggesting that the majority of lead atoms are present in a bulk-like environment (i.e., within $PbBr_6$ octahedra). Like the $^{1}H \rightarrow ^{133}Cs$ correlation experiment, the $^{207}Pb \rightarrow ^{1}H$ 2D NMR spectrum shows correlations to the $-NH_3^+$ and α-CH_2 groups of the oleate and alkylammonium surface ligands.

Given that unique surface signals were only observed for ^{133}Cs, we suspect that the cuboidal $CsPbBr_3$ QDs are primarily terminated by Cs rather than Pb. It is important to keep in mind, however, that surface ^{207}Pb signals may have a large chemical shift anisotropy (CSA) due to asymmetry at the lead coordination environment if $PbBr_5O$, $PbBr_4O_2$, $PbBr_3O_3$, etc. sites were present because of coordination by carboxylate or phosphonate groups. If Pb surface sites with large CSA existed, they would likely have inefficient $^{207}Pb \rightarrow ^{1}H$ cross polarization transfers and would not be detected. One possible solution is to acquire 2D ^{1}H-^{207}Pb correlation spectra with the dipolar heteronuclear multiple quantum coherence (D-HMQC) pulse sequence. D-HMQC experiments work well even when the indirectly detected spin has a large CSA.[57] We were unable to observe any signal using a $^{1}H\{^{207}Pb\}$ D-HMQC experiment, likely because of the small ^{1}H-^{207}Pb dipolar couplings. To definitively probe the composition and structure of the surface, we used $^{1}H\{^{207}Pb\}$ and $^{1}H\{^{133}Cs\}$ RESPDOR experiments[48, 58] to measure dipolar couplings between the surface $-NH_3^+$ protons and proximate surface and sub-surface ^{207}Pb and ^{133}Cs spins (Figure 4). The

heteronuclear dipolar couplings measured by RESPDOR can then be related to inter-nuclear distances. We note that dipolar dephasing experiments such as RESPDOR or REDOR have previously been used to identify and model the structure of surfaces, including determination of ligand binding sites.[59-62] RESPDOR generally shows substantial dipolar dephasing, even when anisotropic interactions broaden the spectrum of the recoupled nucleus beyond detection.[63] In the RESPDOR experiments, only the ^{1}H NMR signal from the ammonium groups of dodecylammonium was monitored because the ammonium groups should sit directly on the surface and have substantial dipole couplings to proximate ^{133}Cs and ^{207}Pb spins on and below the surface. The majority of other ^{1}H spins of the surface ligands will be distant from the surface and have negligible dipole couplings to ^{133}Cs and ^{207}Pb spins. DANTE pulse trains[64, 65] were used to selectively excite the high frequency ammonium ^{1}H NMR signals and suppress other ^{1}H NMR signals. However, alkene ^{1}H NMR signals from oleate and 10-undecenylphosphonate ligands also become increasingly intense as the recoupling time increases and these alkene signals partially overlap with the ammonium group signals (Figure S11 and Figure S12). This signal overlap causes $\Delta S/S_0$ intensities to become smaller than expected at longer recoupling times. Additionally, fluctuations in the MAS frequency will also cause the latter points in the dipolar dephasing curve to exhibit reduced intensity. Hence, fitting of the RESPDOR dipolar dephasing curves focuses on the initial points with total recoupling times of less than 1.5 ms.

Both ^{1}H{^{133}Cs} and ^{1}H{^{207}Pb} RESPDOR experiments show significant dipolar dephasing for the ammonium ^{1}H NMR signal (Figure 4). The dephasing from ^{133}Cs is more significant than that from ^{207}Pb because ^{133}Cs has a natural isotropic abundance of 100%, while the natural isotopic abundance of ^{207}Pb is only 22.1%. However, even taking these differences in isotopic abundance into consideration, the RESPDOR experiments clearly suggest that the surface is Cs terminated, for the reasons described below. In order to fit the RESPDOR dipolar dephasing curves, structural models were constructed by cleaving the known orthorhombic crystal structure of $CsPbBr_3$ parallel to the (010) plane to obtain Cs or Pb terminated slabs (Figure 4B, 4C and 4D, respectively). In the Pb terminated slabs the surface Pb atoms would be capped by the X' ligands (oleic acid or UDPA). A model featuring Cs termination, but with replacement of central and corner Cs atoms by an ammonium, was also considered (Figure 4A). The depth and width of the slabs was restricted to ca. 10 – 12 Å because at these distances the ^{1}H-X dipolar couplings become very weak and make insignificant contributions to the predicted dephasing. The ^{1}H NMR signal of the positively charged ammonium group was monitored in the RESPDOR experiments, therefore the ^{1}H spin in the model slabs is assumed to lie on top of or in between negatively charged Br atoms because such a configuration should maximize favorable electrostatic interactions and minimize energy.

For a given orientation of each slab, ^{133}Cs and ^{207}Pb analytical RESPDOR curves were calculated for each ^{1}H-X spin pair (see SI for details). The total RESPDOR curve was then obtained by taking the product of all dephasing curves for a given orientation of the slab with respect to the external magnetic field.[61, 66, 67] This procedure was then repeated for 200 discrete values of the α, β and γ Euler angles, representing all possible orientations of the slab relative to the magnetic field, to obtain the total powder-averaged RESPDOR curves. To account for the 22.1% natural isotopic abundance of ^{207}Pb, multiple ^{1}H{^{207}Pb} RESPDOR curves were calculated with the numbers of ^{207}Pb spins varying from zero up to the total number of lead atoms (i.e., four Pb atoms, five Pb atoms, and six Pb atoms for structural model 4A, 4B and 4C, respectively). The total dephasing curve was then obtained by summing together all calculated curves, with each curve weighted by the calculated statistical probability of each isotopomer occurring (Table S1-S3).[61]

Among the four models considered, the one that gives the best simultaneous fit of the ^{1}H{^{133}Cs} and ^{1}H{^{207}Pb} RESPDOR curves is obtained with Cs surface termination where the ammonium ^{1}H spin has been substituted at a Cs A-site position (Figure 4A and Figure S13). The substitution of an ammonium group within a pocket of bromide ions created by a Cs vacancy is reasonable considering similar binding sites for alkylammonium ligands are observed in the single crystal X-ray diffraction structures of 2D Ruddlesden-Popper lead halide phases.[68] Kovalenko and co-workers have recently used wide angle total X-ray scattering and TEM to determine that colloidal $CsPbBr_3$ nanoplatelets, different from the cuboidal morphology studied here, are likely CsBr terminated with Cs vacancies.[69] Also, models with alkylammonium ligands substituting into surface Cs sites have previously been considered as one of the most likely surface terminations for $CsPbBr_3$ QDs.[23] In comparison, the Cs-terminated surface without substitution of ammonium into the Cs position gives an adequate fit of the ^{133}Cs dipolar dephasing curve, however, the sub-surface Pb sites are very distant and essentially no ^{207}Pb dipolar dephasing is predicted, in contradiction with the experiment (Figure 4B and Figure S14). Alternatively, if the ^{1}H spin is moved closer to the surface to reproduce the experimental ^{207}Pb dipolar dephasing, then the predicted ^{133}Cs dephasing is overestimated; only with both Cs termination and substitution of Cs for ammonium groups can we simultaneously fit both ^{1}H{^{133}Cs} and ^{1}H{^{207}Pb} RESPDOR curves. Finally, the Pb-terminated surface predicts faster ^{207}Pb dephasing than is observed experimentally and can, therefore, be ruled out as a plausible structural model (Figure 4C and 4D). In summary, the RESPDOR data provides the first experimental evidence for a $[CsPbBr_3](PbBr_2)\{ABr\}$ termination, where the cation A in the outer shell is Cs^+ or dodecylammonium. In this model the anionic oleate or phosphonate ligands are primarily associated with Cs^+ cations in the outer shell. The similarity of the ^{133}Cs and ^{207}Pb NMR spectra and RESPDOR curves for $CsPbBr_3$ QDs with and without UDPA would suggest that there is no major reorganization of the surface caused by ligand exchange of oleate for UDPA, which is consistent with prior results that show neither the Cs:Pb ratio nor the band edge PL emission energy change upon ligand exchange.[20]

The $[CsPbBr_3](PbBr_2)\{ABr\}$ surface model is consistent with a number of other experimental observations. A $CsPbBr_3$ QD with an average edge length of ~10 nm, a Cs-surface termination necessitates Br/Pb and Cs/Pb ratios of ~3.2 and ~1.2, respectively, in agreement with previous experimentally determined values.[21, 22] We note that Cs-surface termination also results in a slight excess of positive charge.[21, 22] Charge compensation should occur through loss of surface Cs, rather than addition of excess Br, because it has been computationally predicted that addition of excess bromide results in low PLQY because of formation of localized trap states above the valance band edge.[21] Finally, solution ^{1}H NMR indicated a dodecylammonium ligand density of 1.0 dodecylammonium nm^{-2}.

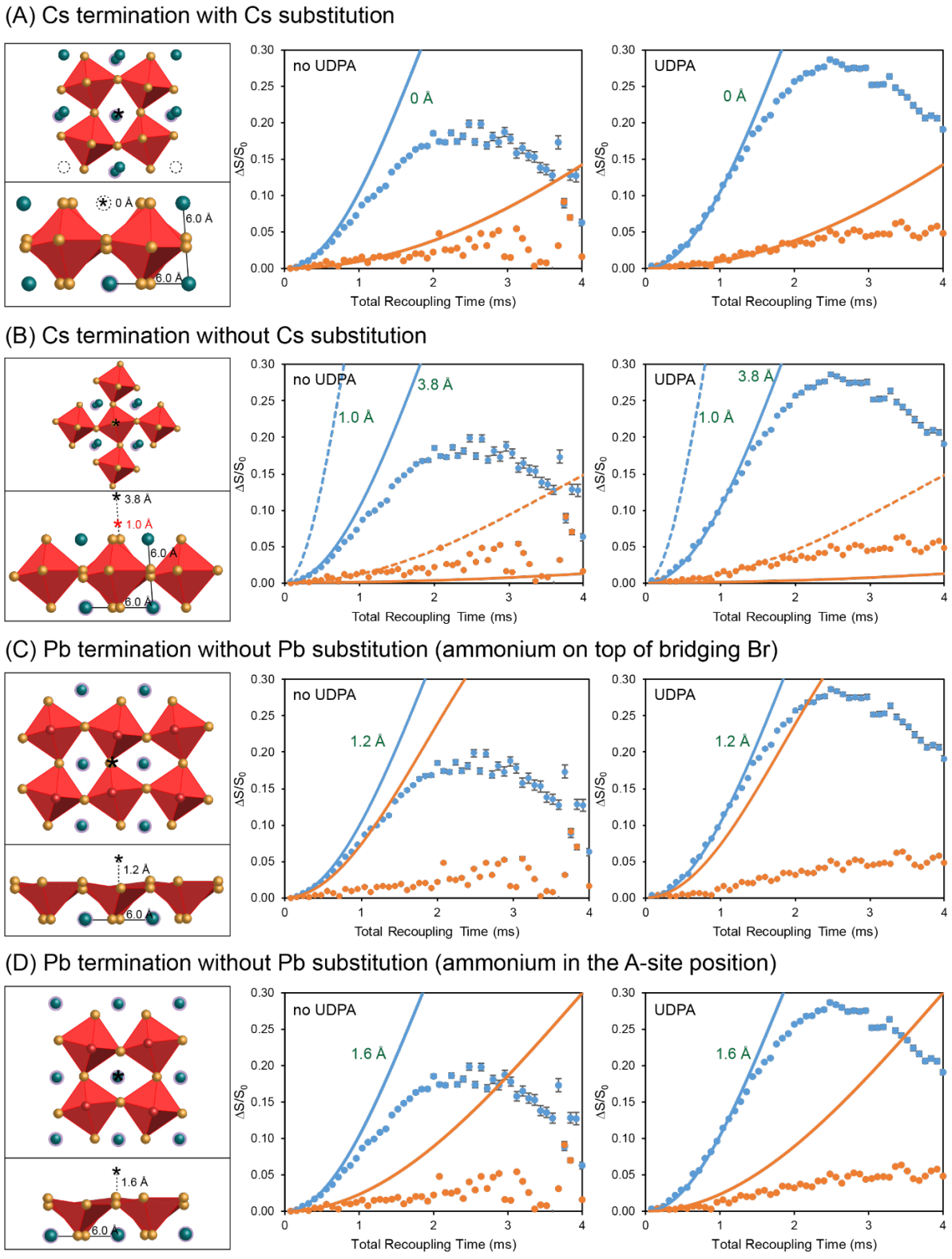

Figure 4. (A, B, C and D) Structural models of the orthorhombic (010) $CsPbBr_3$ surface used to simulate the $^1H\{^{133}Cs\}/^1H\{^{207}Pb\}$ multi-spin RESPDOR curves. Each blue sphere corresponds to a Cs atom while the purple halo around it indicates a Cs atom in the subsurface layer. The ammonium H atom is assumed to be directly above the central atom, in the position indicated by an asterisk. The experimental $\Delta S/S_0$ intensities were plotted as a function of total recoupling time for $CsPbBr_3$ QDs without and with 10-undecenylphosphonate (UDPA) surface ligands. Blue points and orange points correspond to the $^1H\{^{133}Cs\}$ and $^1H\{^{207}Pb\}$ RESPDOR experiments, respectively. Blue and orange lines are simulated dephasing curves for the ^1H-^{133}Cs and ^1H-^{207}Pb spin systems, respectively. The best fit distances are indicated on the plots and structural models.

The model in Figure 4A corresponds to a density of 1.06 dodecylammonium nm^{-2}. The calculated $^{1}H\{^{133}Cs\}$ RESPDOR curves for $[CsPbBr_3](PbBr_2)\{ABr\}$ models are compatible with ligand densities between 0.7 and 2.1 dodecylammonium nm^{-2} (Figure S15), where ligand densities higher than 0.7 dodecylammonium nm^{-2} are achieved by replacing the corner Cs atoms by dodecylammonium ligands as in Figure 4A.

CONCLUSIONS

In summary, we have shown that the surface chemistry of $CsPbBr_3$ QDs can be interrogated by state-of-the-art solid-state NMR experiments. Specifically, we show that dodecylammonium, oleate, and/or 10-undecenylphosphonate are all present as surface ligands. Furthermore, we determine the inter-nuclear distances between dodecylammonium $–NH_3^+$ protons to surface and sub-surface Cs and Pb sites using RESPDOR experiments. Simulation of multi-spin RESPDOR dipolar dephasing curves suggests that the $CsPbBr_3$ QDs are Cs terminated with dodecylammonium ligands substituting into surface Cs A-sites, thereby providing an atomistic picture of QD termination that is $[CsPbBr_3](PbBr_2)\{ABr\}$, where A is Cs or dodecylammonium. These findings are in agreement with the surface-selective ^{207}Pb and ^{133}Cs HETCOR solid-state NMR experiments, as well as previous computational models of QD surfaces.[22] This study demonstrates that solid-state NMR spectroscopy should be useful to better understand how aging of the QDs, ligand exchange, and chemical treatments alter surface structure and affect optical properties. Experiments along these lines are underway. More generally, our results also highlight the utility and future prospects of surface characterization of nanomaterials via solid-state NMR spectroscopy.

EXPERIMENTAL SECTION

General considerations. All syntheses were performed using Schlenk techniques. The QDs were handled in air for isolation and purification and then kept under nitrogen for storage to prevent decomposition. Magic angle spinning (MAS) solid-state NMR experiments were performed with nitrogen gas to limit moisture exposure. Toluene-d_8 (99+%) was purchased from Acros Organics. Cesium carbonate (99.9%), lead (II) bromide (99+%), diphenyl ether (99%), and dodecylamine (98%) were purchased from Alfa Aesar. Oleic acid (90%) was purchased from Sigma Aldrich. 10-Undecylphosphonic acid (98%) was purchased from Gute Chemie. All chemicals were used as received, without further purification.

Synthesis of $CsPbBr_3$ QDs and ligand exchange. $CsPbBr_3$ QDs were synthesized by adapting the procedure outlined by Protesescu *et al.*[1] A Cs(oleate) precursor was generated by adding 101.8 mg (0.3124 mmol) Cs_2CO_3, 5 mL diphenyl ether, and 0.5 mL oleic acid to a 3-neck 25 mL round bottom flask and drying it under vacuum at 60 °C for 1 h. Then, the solution was heated to 120 °C under a nitrogen atmosphere and held for 30 min to ensure complete dissolution of Cs_2CO_3 and conversion to Cs(oleate). The Cs(oleate) solution was subsequently cooled to 100 °C to prepare for hot-injection. A separate solution of $PbBr_2$ (138 mg, 0.376 mmol) and 1 mL oleic acid was dried at 120 °C for 1 h. Diphenyl ether (7.5 mL) and 1 mL dodecylamine were added to the resulting $Pb(oleate)_2$ under a nitrogen atmosphere and were allowed to equilibrate to 120 °C before ramping to 140 °C. The solution of Cs(oleate) (0.8 mL) heated to 100 °C was quickly injected into the $Pb(oleate)_2$ solution at 140 °C; the reaction was allowed to stir for 10 s, and then the reaction was quenched in an ice bath.

To purify the QDs, the thermally quenched suspension was transferred to a centrifuge tube and centrifuged at 6000 rpm for 5 min. The supernatant was discarded, and 5 mL of hexanes was added to the precipitate. To prepare the 10-undecylphosphonic acid-exchanged QDs, 200 μL of 26 mM 10-undecylphosphonic acid (0.0060 g / 1 mL hexanes) was added to the suspension and sonicated for 5 min. For $CsPbBr_3$ QDs without phosphonic acid, no acid was added, but the suspension was still sonicated for 5 min. Approximately 5 mL of isopropanol was added, and the suspension was centrifuged at 6000 rpm for 5 min. The supernatant was discarded, and 5 mL of hexanes was added to the precipitate and sonicated for 5 min. These suspensions were used for TEM and UV-vis/PL measurements and dried overnight for all NMR experiments. Additional details on solution NMR experiments, transmission electron microscopy (TEM), UV-vis spectroscopy, and PXRD are provided in the supporting information.

Solid-state NMR Spectroscopy. All solid-state NMR experiments were performed on a Bruker wide-bore 9.4 T ($\nu_0(^1H)$ = 400 MHz) NMR spectrometer equipped with a Bruker Avance III HD console. All experiments were performed on the 2.5 mm HXY probe, with the exception of $^{1}H\{X\}$ RESPDOR experiments which were performed with a 1.3 mm HX probe. The 2.5 mm and 1.3 mm rotor volumes are about 14 μL and 2 μL, respectively. These volumes correspond to sample weights of approximately 64 mg and 9 mg, respectively. The 2.5 mm HXY MAS probe was configured in ^{1}H-X mode and the X channel could be tuned from ^{13}C to ^{133}Cs. The probe was configured in ^{1}H-^{31}P-^{13}C mode for $^{1}H\rightarrow^{31}P$ 2D CP-HETCOR experiments. A MAS frequency of 25 kHz was used. ^{1}H, ^{13}C and ^{31}P pulse durations and powers were directly optimized on the samples. ^{133}Cs RF pulses were calibrated on CsI. ^{207}Pb RF pulses were calibrated on $Pb(NO_3)_2$. ^{1}H chemical shifts were referenced to neat tetramethylsilane through the use of adamantane ($\delta_{iso}(^1H)$ = 1.82 ppm) as a secondary chemical shift standard. ^{13}C, ^{31}P, ^{133}Cs and ^{207}Pb were directly referenced to the established chemical shift standards using the previously established relative NMR frequencies.[70]

Spin echo,[71] back to back (BABA),[49-51] and dipolar CP-HETCOR with ^{1}H detection[52, 72-75] or direct detection[72] were performed with previously described pulse sequences. The 2D ^{1}H-^{1}H dipolar DQ-SQ experiments were acquired with BABA pulse sequences. The spin echo and BABA experiments were performed with 100 kHz RF fields ^{1}H pulses. The recycle delays, number of scans, and acquisition times for ^{1}H NMR experiments are given in Table S1.

The ^{133}Cs spin echo spectra were acquired with 57 kHz RF field ^{133}Cs pulses. Echo spectra were recorded with both solution (4.4 μs π/2-pulse) and scaled, CT-selective pulse widths (1.1 μs π/2-pulse). However, the same peaks were visible in both sets of spectra, with the solution pulse widths providing approximately three times better sensitivity. Continuous wave decoupling was applied on the ^{1}H channel with an RF field of 100 kHz. The ^{207}Pb spin echo were performed with 100 kHz RF fields ^{207}Pb pulses. The recycle delays, number of scans, and acquisition times for ^{133}Cs and ^{207}Pb NMR experiments are given in Table S1. In all CP experiments the spin lock pulses were linearly ramped from 85% to 100% of the spin lock RF fields,[76] and the direction of the ramp was reversed for the back CP step in proton detected CP-HETCOR experiments. $^{1}H\rightarrow^{13}C$

CPMAS and proton detected CP-HETCOR experiments[52, 73] used ^{1}H $\pi/2$ pulses with 100 kHz RF fields and ^{13}C $\pi/2$ pulses with 109 kHz RF fields. The RF fields for CP matching conditions were experimentally optimized to give maximum signal on each sample. The ^{1}H-^{13}C CP experiments used spin lock pulses with RF fields between 89-92 kHz RF and 109 kHz RF for ^{1}H and ^{13}C, respectively. The contact time was 4 or 5 ms. ^{1}H→^{31}P CP-HETCOR experiments used spin lock pulses with RF fields at 91 kHz RF and 141 kHz RF for ^{1}H and ^{31}P, respectively and contact times were varied from 1 to 9 ms. ^{1}H→^{133}Cs CP-HETCOR experiments used spin lock pulses with RF fields between 84-90 kHz RF and 57 kHz RF for ^{1}H and ^{133}Cs, respectively, and contact times of 2 and 9 ms. Proton detected ^{207}Pb→^{1}H CP-HETCOR experiments used spin lock pulses with RF fields between 94-97 kHz RF and 62 kHz RF for ^{1}H and ^{207}Pb, respectively. SPINAL-64 heteronuclear decoupling was applied with an RF field of ca. 100 kHz for ^{13}C, ^{31}P, and ^{207}Pb NMR experiments.[77] eDUMBO$_{1\text{-}22}$ homonuclear dipolar decoupling[78] was applied during the indirect ^{1}H dimension evolution to improve ^{1}H resolution in the ^{1}H→^{133}Cs and ^{1}H→^{31}P CP-HETCOR experiments. The initial phase and offset of eDUMBO$_{1\text{-}22}$ was optimized directly on each sample and used 32 μs pulse durations and 100 kHz RF fields. The recycle delay, CP contact time, number of scans, number of indirect dimension points and acquisition times for CP-HETCOR experiments are given in Table S1.

RESPDOR experiments[48, 58] with $SR4_1^2$ dipolar recoupling[79] were performed with a Bruker 1.3 mm HX MAS probe was configured in ^{1}H-X mode and the probe was tuned to ^{207}Pb or ^{133}Cs. A 22 pF shunt capacitor was added to the probe to tune down to ^{14}N. An MAS frequency of 50 kHz was used in all cases. ^{1}H RF pulses were directly calibrated on the samples. ^{14}N RF pulses were calibrated on NH_4Cl. DANTE pulse trains[64, 65] were used to selectively excite the high frequency ammonium ^{1}H NMR signals. The DANTE pulse train consisted of 25 pulses which were 0.1 μs in duration with a 100 kHz RF field and 119.9 μs separating each pulse in the train (6 rotor cycles). In the RESPDOR experiments, ^{1}H spectra with varying recoupling time were acquired with (S) and without (S_0) the application of a dephasing pulse on the heteronucleus. The duration of dipolar recoupling was incremented in a linear manner. For ^{14}N and ^{133}Cs, a saturation pulse with a duration of 1.5 times rotor cycles and a 79 kHz RF field was centered on the ^{1}H refocusing π-pulse. The ^{14}N/^{133}Cs RF fields were experimentally optimized to give maximum saturation on each sample. For ^{1}H{^{207}Pb} RESPDOR experiments, dephasing was induced by ^{207}Pb π pulses with a 125 kHz RF field (4 μs π-pulse). The recoupling curves were obtained by plotting $\Delta S/S_0$ as a function of the recoupling time and were fitted using an in-house C program as described in the Supporting Information.

ASSOCIATED CONTENT

The Supporting Information is available free of charge and includes additional experimental details, optical measurements, TEM/SEM-EDS micrographs, powder XRD patterns, ^{1}H solution NMR and additional solid-state NMR spectra.

AUTHOR INFORMATION

Corresponding Author

*(AJR) E-mail: arossini@iastate.edu, Phone: 515-294-8952

*(RLB) E-mail: brutchey@usc.edu, Phone: 213-821-2554

ACKNOWLEDGMENT

Solid-state NMR experiments and data analysis (YC, FP, and AJR) were supported by the U.S. Department of Energy (DOE), Office of Science, Basic Energy Sciences, Materials Science and Engineering Division. AHF is grateful to the U.S. Department of Energy Office of Science Undergraduate Laboratory Internship (SULI) program for the assistantship and opportunity to participate in the SULI program. The Ames Laboratory is operated for the U.S. DOE by Iowa State University under contract # DE-AC02-07CH11358. The quantum dot synthesis and surface chemistry were supported by the U.S. Department of Energy, Office of Science, Basic Energy Sciences, under Award # DE−FG02−11ER46826 to RLB. SRS acknowledges support from the Graduate Research Fellowship Program of the National Science Foundation. We are grateful to Prof. Javier Vela (ISU and Ames Laboratory) for providing access to the glovebox used to pack rotors and store samples.

REFERENCES

(1) Protesescu, L.; Yakunin, S.; Bodnarchuk, M. I.; Krieg, F.; Caputo, R.; Hendon, C. H.; Yang, R. X.; Walsh, A.; Kovalenko, M. V., Nanocrystals of Cesium Lead Halide Perovskites ($CsPbX_3$, X = Cl, Br, and I): Novel Optoelectronic Materials Showing Bright Emission with Wide Color Gamut. *Nano Lett.* **2015,** *15* (6), 3692-3696.
(2) Kovalenko, M. V.; Protesescu, L.; Bodnarchuk, M. I., Properties and potential optoelectronic applications of lead halide perovskite nanocrystals. *Science* **2017,** *358* (6364), 745-750.
(3) Huang, H.; Bodnarchuk, M. I.; Kershaw, S. V.; Kovalenko, M. V.; Rogach, A. L., Lead Halide Perovskite Nanocrystals in the Research Spotlight: Stability and Defect Tolerance. *ACS Energy Lett.* **2017,** *2* (9), 2071-2083.
(4) Lin, K. B.; Xing, J.; Quan, L. N.; de Arquer, F. P. G.; Gong, X. W.; Lu, J. X.; Xie, L. Q.; Zhao, W. J.; Zhang, D.; Yan, C. Z.; Li, W. Q.; Liu, X. Y.; Lu, Y.; Kirman, J.; Sargent, E. H.; Xiong, Q. H.; Wei, Z. H., Perovskite light-emitting diodes with external quantum efficiency exceeding 20 per cent. *Nature* **2018,** *562* (7726), 245–248.
(5) Wei, Z. H.; Xing, J., The Rise of Perovskite Light-Emitting Diodes. *J. Phys. Chem. Lett.* **2019,** *10* (11), 3035-3042.
(6) Lu, M.; Zhang, Y.; Wang, S. X.; Guo, J.; Yu, W. W.; Rogach, A. L., Metal Halide Perovskite Light-Emitting Devices: Promising Technology for Next-Generation Displays. *Adv. Funct. Mater.* **2019,** *29* (30), 1902008.
(7) Tai, Q. D.; Tang, K. C.; Yan, F., Recent progress of inorganic perovskite solar cells. *Energy Environ. Sci.* **2019,** *12* (8), 2375-2405.
(8) Wang, K. Y.; Wang, S.; Xiao, S. M.; Song, Q. H., Recent Advances in Perovskite Micro- and Nanolasers. *Adv. Opt. Mater.* **2018,** *6* (18), 1800278.
(9) Hao, M.; Bai, Y.; Zeiske, S.; Ren, L.; Liu, J.; Yuan, Y.; Zarrabi, N.; Cheng, N.; Ghasemi, M.; Chen, P.; Lyu, M.; He, D.; Yun, J.-H.; Du, Y.; Wang, Y.; Ding, S.; Armin, A.; Meredith, P.; Liu, G.; Cheng, H.-M.; Wang, L., Ligand-assisted cation-exchange engineering for high-efficiency colloidal Cs1−xFAxPbI3 quantum dot solar cells with reduced phase segregation. *Nat. Energy* **2020,** *5* (1), 79-88.
(10) Brutchey, R.; Hens, Z.; Kovalenko, M. V., Surface Chemistry of Colloidal Semiconductor Nanocrystals: Organic, Inorganic, and Hybrid. *Chemistry of Organo‐Hybrids* **2014**, 233-271.

(11) Owen, J., The coordination chemistry of nanocrystal surfaces. *Science* **2015,** *347* (6222), 615-616.
(12) Pan, J.; Shang, Y. Q.; Yin, J.; De Bastiani, M.; Peng, W.; Dursun, I.; Sinatra, L.; El-Zohry, A. M.; Hedhili, M. N.; Emwas, A. H.; Mohammed, O. F.; Ning, Z. J.; Bakr, O. M., Bidentate Ligand-Passivated CsPbI3 Perovskite Nanocrystals for Stable Near-Unity Photoluminescence Quantum Yield and Efficient Red Light-Emitting Diodes. *J. Am. Chem. Soc.* **2018,** *140* (2), 562-565.
(13) Pan, J.; Quan, L. N.; Zhao, Y. B.; Peng, W.; Murali, B.; Sarmah, S. P.; Yuan, M. J.; Sinatra, L.; Alyami, N. M.; Liu, J. K.; Yassitepe, E.; Yang, Z. Y.; Voznyy, O.; Comin, R.; Hedhili, M. N.; Mohammed, O. F.; Lu, Z. H.; Kim, D. H.; Sargent, E. H.; Bakr, O. M., Highly Efficient Perovskite-Quantum-Dot Light-Emitting Diodes by Surface Engineering. *Adv. Mater.* **2016,** *28* (39), 8718-8725.
(14) Akkerman, Q. A.; Raino, G.; Kovalenko, M. V.; Manna, L., Genesis, challenges and opportunities for colloidal lead halide perovskite nanocrystals. *Nat. Mater.* **2018,** *17* (5), 394-405.
(15) Chen, B.; Rudd, P. N.; Yang, S.; Yuan, Y.; Huang, J., Imperfections and their passivation in halide perovskite solar cells. *Chem. Soc. Rev.* **2019,** *48* (14), 3842-3867.
(16) Pan, J.; Sarmah, S. P.; Murali, B.; Dursun, I.; Peng, W.; Parida, M. R.; Liu, J.; Sinatra, L.; Alyami, N.; Zhao, C.; Alarousu, E.; Ng, T. K.; Ooi, B. S.; Bakr, O. M.; Mohammed, O. F., Air-Stable Surface-Passivated Perovskite Quantum Dots for Ultra-Robust, Single- and Two-Photon-Induced Amplified Spontaneous Emission. *J. Phys. Chem. Lett.* **2015,** *6* (24), 5027-5033.
(17) Wheeler, L. M.; Sanehira, E. M.; Marshall, A. R.; Schulz, P.; Suri, M.; Anderson, N. C.; Christians, J. A.; Nordlund, D.; Sokaras, D.; Kroll, T.; Harvey, S. P.; Berry, J. J.; Lin, L. Y.; Luther, J. M., Targeted Ligand-Exchange Chemistry on Cesium Lead Halide Perovskite Quantum Dots for High-Efficiency Photovoltaics. *J. Am. Chem. Soc.* **2018,** *140* (33), 10504-10513.
(18) Ravi, V. K.; Santra, P. K.; Joshi, N.; Chugh, J.; Singh, S. K.; Rensmo, H.; Ghosh, P.; Nag, A., Origin of the Substitution Mechanism for the Binding of Organic Ligands on the Surface of $CsPbBr_3$ Perovskite Nanocubes. *J. Phys. Chem. Lett.* **2017,** *8* (20), 4988-4994.
(19) De Roo, J.; Ibanez, M.; Geiregat, P.; Nedelcu, G.; Walravens, W.; Maes, J.; Martins, J. C.; Van Driessche, I.; Koyalenko, M. V.; Hens, Z., Highly Dynamic Ligand Binding and Light Absorption Coefficient of Cesium Lead Bromide Perovskite Nanocrystals. *ACS Nano* **2016,** *10* (2), 2071-2081.
(20) Smock, S. R.; Williams, T. J.; Brutchey, R. L., Quantifying the Thermodynamics of Ligand Binding to $CsPbBr_3$ Quantum Dots. *Angew. Chem. Int. Ed.* **2018,** *57* (36), 11711-11715.
(21) ten Brinck, S.; Infante, I., Surface Termination, Morphology, and Bright Photoluminescence of Cesium Lead Halide Perovskite Nanocrystals. *ACS Energy Lett.* **2016,** *1* (6), 1266-1272.
(22) Bodnarchuk, M. I.; Boehme, S. C.; ten Brinck, S.; Bernasconi, C.; Shynkarenko, Y.; Krieg, F.; Widmer, R.; Aeschlimann, B.; Gunther, D.; Kovalenko, M. V.; Infante, I., Rationalizing and Controlling the Surface Structure and Electronic Passivation of Cesium Lead Halide Nanocrystals. *ACS Energy Lett.* **2019,** *4* (1), 63-74.
(23) Almeida, G.; Infante, I.; Manna, L., Resurfacing halide perovskite nanocrystals. *Science* **2019,** *364* (6443), 833-834.
(24) Loyingood, D. D.; Achey, R.; Paravastu, A. K.; Strouse, G. F., Size- and Site-Dependent Reconstruction in CdSe QDs Evidenced by $^{77}Se\{^{1}H\}$ CP-MAS NMR Spectroscopy. *J. Am. Chem. Soc.* **2010,** *132* (10), 3344-3354.
(25) Virieux, H.; Le Troedec, M.; Cros-Gagneux, A.; Ojo, W. S.; Delpech, F.; Nayral, C.; Martinez, H.; Chaudret, B., InP/ZnS Nanocrystals: Coupling NMR and XPS for Fine Surface and Interface Description. *J. Am. Chem. Soc.* **2012,** *134* (48), 19701-19708.
(26) Hanrahan, M. P.; Fought, E. L.; Windus, T. L.; Wheeler, L. M.; Anderson, N. C.; Neale, N. R.; Rossini, A. J., Characterization of Silicon Nanocrystal Surfaces by Multidimensional Solid-State NMR Spectroscopy. *Chem. Mater.* **2017,** *29* (24), 10339-10351.
(27) Cadars, S.; Smith, B. J.; Epping, J. D.; Acharya, S.; Belman, N.; Golan, Y.; Chmelka, B. F., Atomic Positional Versus Electronic Order in Semiconducting ZnSe Nanoparticles. *Phys. Rev. Lett.* **2009,** *103* (13), 136802.
(28) Wang, R. B.; Ratcliffe, C. I.; Wu, X. H.; Voznyy, O.; Tao, Y.; Yu, K., Magic-Sized Cd_3P_2 II-V Nanoparticles Exhibiting Bandgap Photoemission. *J. Phys. Chem. C* **2009,** *113* (42), 17979-17982.
(29) Yesinowski, J. P., Solid-State NMR of Inorganic Semiconductors. *Top Curr Chem* **2012,** *306*, 229-312.
(30) Bernard, G. M.; Wasylishen, R. E.; Ratcliffe, C. I.; Terskikh, V.; Wu, Q.; Buriak, J. M.; Hauger, T., Methylammonium Cation Dynamics in Methylammonium Lead Halide Perovskites: A Solid-State NMR Perspective. *J. Phys. Chem. A* **2018,** *122* (6), 1560-1573.
(31) Karmakar, A.; Askar, A. M.; Bernard, G. M.; Terskikh, V. V.; Ha, M.; Patel, S.; Shankar, K.; Michaelis, V. K., Mechanochemical Synthesis of Methylammonium Lead Mixed-Halide Perovskites: Unraveling the Solid-Solution Behavior Using Solid-State NMR. *Chem. Mater.* **2018,** *30* (7), 2309-2321.
(32) Franssen, W. M. J.; van Es, S. G. D.; Dervisoglu, R.; de Wijs, G. A.; Kentgens, A. P. M., Symmetry, Dynamics, and Defects in Methylammonium Lead Halide Perovskites. *J. Phys. Chem. Lett.* **2017,** *8* (1), 61-66.
(33) Knop, O.; Wasylishen, R. E.; White, M. A.; Cameron, T. S.; Vanoort, M. J. M., Alkylammonium Lead Halides. 2. $CH_3NH_3PbCl_3$, $CH_3NH_3PbBr_3$, $CH_3NH_3PbI_3$ Perovskites - Cuboctahedral Halide Cages with Isotropic Cation Reorientation. *Can. J. Chem.* **1990,** *68* (3), 412-422.
(34) Xu, Q.; Eguchi, T.; Nakayama, H.; Nakamura, N.; Kishita, M., Molecular Motions and Phase-Transitions in Solid $CH_3NH_3PbCl_3$, $CH_3NH_3PbBr_3$, $CH_3NH_3PbI_3$, as Studied by NMR and NQR. *Z Naturforsch A* **1991,** *46* (3), 240-246.
(35) Fabini, D. H.; Siaw, T. A.; Stoumpos, C. C.; Laurita, G.; Olds, D.; Page, K.; Hu, J. G.; Kanatzidis, M. G.; Han, S.; Seshadri, R., Universal Dynamics of Molecular Reorientation in Hybrid Lead Iodide Perovskites. *J. Am. Chem. Soc.* **2017,** *139* (46), 16875-16884.
(36) Kubicki, D. J.; Prochowicz, D.; Hofstetter, A.; Zakeeruddin, S. M.; Gratzel, M.; Emsley, L., Phase Segregation in Cs-, Rb- and K-Doped Mixed-Cation $MA_xFA_{1-x}PbI_3$ Hybrid Perovskites from Solid-State NMR. *J. Am. Chem. Soc.* **2017,** *139* (40), 14173-14180.
(37) Rosales, B. A.; Men, L.; Cady, S. D.; Hanrahan, M. P.; Rossini, A. J.; Vela, J., Persistent Dopants and Phase Segregation in Organolead Mixed-Halide Perovskites. *Chem. Mater.* **2016,** *28* (19), 6848-6859.

(38) Kubicki, D. J.; Prochowicz, D.; Hofstetter, A.; Pechy, P.; Zakeeruddin, S. M.; Gratzel, M.; Emsley, L., Cation Dynamics in Mixed-Cation $MA_xFA_{1-x}PbI_3$ Hybrid Perovskites from Solid-State NMR. *J. Am. Chem. Soc.* **2017,** *139* (29), 10055-10061.
(39) Rosales, B. A.; Hanrahan, M. P.; Boote, B. W.; Rossini, A. J.; Smith, E. A.; Vela, J., Lead Halide Perovskites: Challenges and Opportunities in Advanced Synthesis and Spectroscopy. *ACS Energy Lett.* **2017,** *2* (4), 906-914.
(40) Hanrahan, M. P.; Men, L.; Rosales, B. A.; Vela, J.; Rossini, A. J., Sensitivity-Enhanced ^{207}Pb Solid-State NMR Spectroscopy for the Rapid, Non-Destructive Characterization of Organolead Halide Perovskites. *Chem. Mater.* **2018,** *30* (20), 7005-7015.
(41) Askar, A. M.; Bernard, G. M.; Wiltshire, B.; Shankar, K.; Michaelis, V. K., Multinuclear Magnetic Resonance Tracking of Hydro, Thermal, and Hydrothermal Decomposition of $CH_3NH_3PbI_3$. *J. Phys. Chem. C* **2017,** *121* (2), 1013-1024.
(42) Karmakar, A.; Dodd, M. S.; Zhang, X. Y.; Oakley, M. S.; Klobukowski, M.; Michaelis, V. K., Mechanochemical synthesis of 0D and 3D cesium lead mixed halide perovskites. *Chem. Commun.* **2019,** *55* (35), 5079-5082.
(43) Piveteau, L.; Ong, T.-C.; Rossini, A. J.; Emsley, L.; Coperet, C.; Kovalenko, M. V., Structure of colloidal quantum dots from dynamic nuclear polarization surface enhanced NMR spectroscopy. *J. Am. Chem. Soc.* **2015,** *137* (43), 13964-13971.
(44) Brown, A. A.; Hooper, T. J.; Veldhuis, S. A.; Chin, X. Y.; Bruno, A.; Vashishtha, P.; Tey, J. N.; Jiang, L.; Damodaran, B.; Pu, S. H., Self-assembly of a robust hydrogen-bonded octylphosphonate network on cesium lead bromide perovskite nanocrystals for light-emitting diodes. *Nanoscale* **2019,** *11* (25), 12370-12380.
(45) Antanovich, A.; Prudnikau, A.; Matsukovich, A.; Achtstein, A.; Artemyev, M., Self-assembly of CdSe nanoplatelets into stacks of controlled size induced by ligand exchange. *J. Phys. Chem. C* **2016,** *120* (10), 5764-5775.
(46) Cottingham, P.; Brutchey, R. L., On the crystal structure of colloidally prepared $CsPbBr_3$ quantum dots. *Chem. Commun.* **2016,** *52* (30), 5246-5249.
(47) Brennan, M. C.; Herr, J. E.; Nguyen-Beck, T. S.; Zinna, J.; Draguta, S.; Rouvimov, S.; Parkhill, J.; Kuno, M., Origin of the Size-Dependent Stokes Shift in $CsPbBr_3$ Perovskite Nanocrystals. *J. Am. Chem. Soc.* **2017,** *139* (35), 12201-12208.
(48) Gan, Z. H., Measuring multiple carbon-nitrogen distances in natural abundant solids using R-RESPDOR NMR. *Chem. Commun.* **2006,** (45), 4712-4714.
(49) Feike, M.; Demco, D. E.; Graf, R.; Gottwald, J.; Hafner, S.; Spiess, H. W., Broadband multiple-quantum NMR spectroscopy. *J. Magn. Reson.* **1996,** *122* (2), 214-221.
(50) Schnell, I.; Lupulescu, A.; Hafner, S.; Demco, D. E.; Spiess, H. W., Resolution enhancement in multiple-quantum MAS NMR spectroscopy. *J. Magn. Reson.* **1998,** *133* (1), 61-69.
(51) Schnell, I., Dipolar recoupling in fast-MAS solid-state NMR spectroscopy. *Prog. Nucl. Magn. Reson. Spectrosc.* **2004,** *45* (1-2), 145-207.
(52) Wiench, J. W.; Bronnimann, C. E.; Lin, V. S. Y.; Pruski, M., Chemical shift correlation NMR spectroscopy with indirect detection in fast rotating solids: Studies of organically functionalized mesoporous silicas. *J. Am. Chem. Soc.* **2007,** *129* (40), 12076-12077.
(53) Thomas, L. C., *The Identification of Functional Groups in Organophosphorus Compounds*. Academic Press: 1974.
(54) Crutchfield, M. M.; Griffith, E. J.; Grayson, M., *Topics in phosphorus chemistry. Vol. 5, Vol. 5*. Interscience: New York, 1967.
(55) Holland, G. P.; Sharma, R.; Agola, J. O.; Amin, S.; Solomon, V. C.; Singh, P.; Buttry, D. A.; Yarger, J. L., NMR Characterization of Phosphonic Acid Capped SnO2 Nanoparticles. *Chem. Mater.* **2007,** *19* (10), 2519-2526.
(56) Kubicki, D. J.; Prochowicz, D.; Pinon, A.; Stevanato, G.; Hofstetter, A.; Zakeeruddin, S. M.; Gratzel, M.; Emsley, L., Doping and phase segregation in Mn^{2+} and Co^{2+} doped lead halide perovskites from ^{133}Cs and ^{1}H NMR relaxation enhancement. *J. Mater. Chem. A* **2019,** *7* (5), 2326-2333.
(57) Rossini, A. J.; Hanrahan, M. P.; Thuo, M., Rapid acquisition of wideline MAS solid-state NMR spectra with fast MAS, proton detection, and dipolar HMQC pulse sequences. *Phys. Chem. Chem. Phys.* **2016,** *18* (36), 25284-25295.
(58) Chen, L.; Wang, Q. A.; Hu, B. W.; Lafon, O.; Trebosc, J.; Deng, F.; Amoureux, J. P., Measurement of hetero-nuclear distances using a symmetry-based pulse sequence in solid-state NMR. *Phys. Chem. Chem. Phys.* **2010,** *12* (32), 9395-9405.
(59) Perras, F. A.; Padmos, J. D.; Johnson, R. L.; Wang, L. L.; Schwartz, T. J.; Kobayashi, T.; Horton, J. H.; Dumesic, J. A.; Shanks, B. H.; Johnson, D. D.; Pruski, M., Characterizing Substrate-Surface Interactions on Alumina-Supported Metal Catalysts by Dynamic Nuclear Polarization-Enhanced Double-Resonance NMR Spectroscopy. *J. Am. Chem. Soc.* **2017,** *139* (7), 2702-2709.
(60) Hu, Y. Y.; Rawal, A.; Schmidt-Rohr, K., Strongly bound citrate stabilizes the apatite nanocrystals in bone. *Proc. Natl. Acad. Sci. U. S. A.* **2010,** *107* (52), 22425-22429.
(61) Perras, F. A.; Wang, Z. C.; Kobayashi, T.; Baiker, A.; Huang, J.; Pruski, M., Shedding light on the atomic-scale structure of amorphous silica-alumina and its Bronsted acid sites. *Phys. Chem. Chem. Phys.* **2019,** *21* (35), 19529-19537.
(62) Berruyer, P.; Lelli, M.; Conley, M. P.; Silverio, D. L.; Widdifield, C. M.; Siddiqi, G.; Gajan, D.; Lesage, A.; Copéret, C.; Emsley, L., Three-Dimensional Structure Determination of Surface Sites. *J. Am. Chem. Soc.* **2017,** *139* (2), 849-855.
(63) Nagarkar, S. S.; Kurasho, H.; Duong, N. T.; Nishiyama, Y.; Kitagawa, S.; Horike, S., Crystal melting and glass formation in copper thiocyanate based coordination polymers. *Chem. Commun.* **2019,** *55* (38), 5455-5458.
(64) Bodenhausen, G.; Freeman, R.; Morris, G. A., Simple Pulse Sequence for Selective Excitation in Fourier-Transform Nmr. *J. Magn. Reson.* **1976,** *23* (1), 171-175.
(65) Morris, G. A.; Freeman, R., Selective Excitation in Fourier-Transform Nuclear Magnetic-Resonance. *J. Magn. Reson.* **1978,** *29* (3), 433-462.
(66) Goetz, J. M.; Schaefer, J., REDOR dephasing by multiple spins in the presence of molecular motion. *J. Magn. Reson.* **1997,** *127* (2), 147-154.
(67) Lu, X. Y.; Lafon, O.; Trebosc, J.; Amoureux, J. P., Detailed analysis of the S-RESPDOR solid-state NMR method for inter-nuclear distance measurement between spin-1/2 and quadrupolar nuclei. *J. Magn. Reson.* **2012,** *215*, 34-49.
(68) Stoumpos, C. C.; Cao, D. H.; Clark, D. J.; Young, J.; Rondinelli, J. M.; Jang, J. I.; Hupp, J. T.; Kanatzidis, M. G., Ruddlesden–Popper Hybrid Lead Iodide Perovskite 2D

Homologous Semiconductors. *Chem. Mater.* **2016,** *28* (8), 2852-2867.
(69) Bertolotti, F.; Nedelcu, G.; Vivani, A.; Cervellino, A.; Masciocchi, N.; Guagliardi, A.; Kovalenko, M. V., Crystal Structure, Morphology, and Surface Termination of Cyan-Emissive, Six-Monolayers-Thick $CsPbBr_3$ Nanoplatelets from X-ray Total Scattering. *Acs Nano* **2019**.
(70) Harris, R. K.; Becker, E. D.; De Menezes, S. M. C.; Goodfellow, R.; Granger, P., NMR nomenclature. Nuclear spin properties and conventions for chemical shifts - (IUPAC recommendations 2001). *Pure Appl. Chem.* **2001,** *73* (11), 1795-1818.
(71) Hahn, E. L., Spin Echoes. *Phys. Rev.* **1950,** *77* (5), 746-746.
(72) Roberts, J. E.; Vega, S.; Griffin, R. G., Two-Dimensional Heteronuclear Chemical-Shift Correlation Spectroscopy in Rotating Solids. *J. Am. Chem. Soc.* **1984,** *106* (9), 2506-2512.
(73) Ishii, Y.; Tycko, R., Sensitivity enhancement in solid state ^{15}N NMR by indirect detection with high-speed magic angle spinning. *J. Magn. Reson.* **2000,** *142* (1), 199-204.
(74) Ishii, Y.; Yesinowski, J. P.; Tycko, R., Sensitivity enhancement in solid-state ^{13}C NMR of synthetic polymers and biopolymers by ^{1}H NMR detection with high-speed magic angle spinning. *J. Am. Chem. Soc.* **2001,** *123* (12), 2921-2922.
(75) Zhou, D. H.; Rienstra, C. M., Rapid analysis of organic compounds by proton-detected heteronuclear correlation NMR spectroscopy with 40 kHz magic-angle spinning. *Angew. Chem. Int. Ed.* **2008,** *47* (38), 7328-7331.
(76) Metz, G.; Wu, X. L.; Smith, S. O., Ramped-Amplitude Cross-Polarization in Magic-Angle-Spinning Nmr. *J. Magn. Reson.* **1994,** *110* (2), 219-227.
(77) Fung, B. M.; Khitrin, A. K.; Ermolaev, K., An improved broadband decoupling sequence for liquid crystals and solids. *J. Magn. Reson.* **2000,** *142* (1), 97-101.
(78) Sakellariou, D.; Lesage, A.; Hodgkinson, P.; Emsley, L., Homonuclear dipolar decoupling in solid-state NMR using continuous phase modulation. *Chem. Phys. Lett.* **2000,** *319* (3-4), 253-260.
(79) Brinkmann, A.; Kentgens, A. P. M., Proton-selective ^{17}O-^{1}H distance measurements in fast magic-angle-spinning solid-state NMR spectroscopy for the determination of hydrogen bond lengths. *J. Am. Chem. Soc.* **2006,** *128* (46), 14758-14759.

Table of Contents Graphic